Experimental and 0D Numerical Investigation of Ultra-Lean Combustion Concept to Improve the Efficiency of SI Engine

Vincenzo de Bellis, Enrica Malfi, Fabio Bozza, Deepak Kumar, David Serrano, Alessio Dulbecco, Jean-Marc Zaccardi

2021-01-0384 Published 06 Apr 2021

Experimental and 0D Numerical Investigation of Ultra-Lean Combustion Concept to Improve the Efficiency of SI Engine

Vincenzo De Bellis, Enrica Malfi, and Fabio Bozza University of Naples Federico II

Deepak Kumar, David Serrano, Alessio Dulbecco, and Jean-Marc Zaccardi IFP Energies Nouvelles, Ins. Carnot IFPEN Transports Energie

Citation: De Bellis, V., Malfi, E., Bozza, F., Kumar, D. et al., "Experimental and 0D Numerical Investigation of Ultra-Lean Combustion Concept to Improve the Efficiency of SI Engine," SAE Technical Paper 2021-01-0384, 2021, doi:10.4271/2021-01-0384.

Abstract

Recently, the car manufacturers are moving towards innovative Spark Ignition (SI) engine architectures with unconventional combustion concepts, aiming to comply with the stringent regulation imposed by EU and other legislators. The introduction of burdensome cycles for vehicle homologation, indeed, requires an engine characterized by a high efficiency in the most of its operating conditions, for which a conventional SI engine results to be ineffective. Combustion systems which work with very lean air/fuel mixture have demonstrated to be a promising solution to this concern. Higher specific heat ratio, minor heat losses and increased knock resistance indeed allow improving fuel consumption. Additionally, the lower combustion temperatures enable to reduce NO_X production.

Since conventional SI engines can work with a limited amount of excess air, alternative solutions are being developed to overcome this constraint and reach the above benefit. Among all these solutions, replacing the spark-plug with a Pre-Chamber (PC) ignition system is gaining increasing interest. For this architecture, the combustion process starts in the PC and propagates in the main-chamber in the form of multiple turbulent jets of hot gas, with high-turbulence level. This ensures stable flame propagation even under extremely lean mixtures.

In this research activity, an ultra-lean PC SI engine is numerically and experimentally investigated to assess the potential improvement of the thermal efficiency for ultra-lean operations. To this aim, a research single cylinder engine, fuelled with gasoline, is tested at fixed load and speed, realizing an air / fuel ratio sweep. A 1D/0D model of the examined engine is implemented in a commercial modelling framework (GT-Power™), where "in-house developed" sub-models are embedded, simulating in-cylinder phenomena, such as combustion, turbulence, heat transfer and pollutant emissions.

The numerical approach, preliminarily tuned against 3D simulations and experimental outcomes, demonstrated to accurately reproduce the engine behaviour, without requiring any case-dependent tuning of the model constants. Both numerical and experimental results proved that working in ultra-lean condition allows to significantly improve the indicated thermal efficiency, abating the NOx emissions, while penalizing the HC production.

Introduction

It is now urgent to reduce much faster the transport related fossil CO_2 emissions in order to keep hoping in the achievement of a <2°C global warming scenario. In Europe for example, tank-to-wheel CO_2 emissions of road transport should be reduced by 69% by 2050 based on 2010 emissions (and even by 90% according to the European Green Deal) [1].

The continuous improvement of Internal Combustion Engines (ICEs) will support the industry in achieving this crucial objective by contributing to minimize the overall energy consumption of future hybrid vehicles that should represent more than 30% of the total worldwide sales in 2030 [2,3,4] even if some local variability is to be expected because of future national regulations and incentives.

Electrified powertrains impose specific requirements for the ICE. These will only have a limited operating range while providing however very high efficiencies (>50%) in order to lower also the vehicle energy consumption even in highway driving conditions where hybridization usually does not bring any major benefit. In parallel, ICE-powered vehicles will have to comply with strict regulations even for still non-regulated emissions in order to safeguard real-world driving emissions and to achieve a "near zero" impact on air quality in particular for vehicles operating in urban environments.

Regarding Spark-Ignition (SI) ICE, downsized architectures with VVT/VVA devices and turbocharging are now state-of-the-art [5]. Several approaches are possible to increase the thermal efficiency and some benefits can be obtained using advanced anti-knock measures, such as variable compression ratio [6], cooled exhaust gas recirculation [7], water injection [8], and passive Pre-Chamber (PC) ignition [9]. Long strokes combined with high compression ratios can also offer

further benefits [10], but in the end the fuel consumption advantages of all stoichiometric approaches are still rather limited when vehicles are tested over WLTC [11].

A significant improvement in efficiency can be expected by combining the above-mentioned measures with air dilution of the air/fuel mixture. Several publicly and privately funded research projects have been launched to develop so called "super-lean" or "ultra-lean" spark-ignited engines as they really represent a promising solution [12,13]. Thanks to this air dilution, the mixture heat capacity and the ratio of its specific heats can be increased which leads to a better knock resistance, possibly also with high compression ratios, and to a higher thermal efficiency. Fuel consumption can also be lowered at low load since the throttling losses can be reduced. In ultra-lean conditions, raw NOx emissions are decreased thanks to lower combustion temperatures [14,15], and raw CO emissions are also lowered. The impact of lean combustion on unburned hydrocarbon (uHC) emissions is not as straightforward: the excess air should theoretically support the fuel oxidation process with limited dilutions, but local flame quenching is the dominating effect in ultra-lean conditions resulting in a potential increase in uHC emissions.

However, conventional SI ICEs running on standard gasoline fuel do only tolerate a moderate dilution, reducing thus the real advantage of lean-burn combustion [16]. An overall dedicated combustion system is required for ultra-lean operation, especially concerning the ignition system which must be reliable in order to support lambda control and ignition close to unstable conditions. Several solutions have been investigated in the recent years to extend this dilution limit. Moriyoshi et al. [17] showed that a slight vertical fuel stratification could limit the bulk flame quenching and reduce the cycle-to-cycle fluctuations, which are typical for the combustion of lean air/fuel mixtures. High energy ignition systems can also be used such as corona ignition systems, laser ignition or microwave ignition [18,19,20]. Alternatively, the recent literature shows that the requirements for some lean burn concepts such as spark controlled compression ignition can be completely different as the ignition and the main combustion phase are strongly supported by auto-ignition [21].

Active pre-chamber ignition is another possibility to efficiently provide the necessary ignition energy to large volumes in ultra-lean conditions [18,22,23]. Contrary to passive PC, the active one is supplied with fuel separately from the Main-Chamber (MC), which gives the opportunity to prepare a stoichiometric mixture in the PC and a lean mixture in the MC, both volumes being connected through small orifices. Combustion starts at the spark-plug located in the PC, and then turbulent jets of hot gases are expelled from the PC towards the MC, increasing the turbulence of the cylinder charge and allowing the spatial ignition of extremely lean mixtures. This method enhances the burn rate and improves the combustion stability [24].

Various experimental activities have already been carried out with active pre-chambers in the recent years either to assess the maximal lean limit of different PCs and engines configurations, or to identify the most suitable fuel to be injected into the PC [18, 25,26,27,28], knowing that standard gasoline fuel is still the most relevant option given the current fuel supply infrastructure worldwide and the customer expectations. Several key challenges still remain however in order to optimize on the one hand the scavenging, charge motion and mixture preparation in the pre-chamber, and on the other hand the resulting spatial ignition process in the MC.

To accurately study the synergies of combustion, chemical kinetics and turbulence in a pre-chamber engine, the most suitable numerical tools are 3D CFD simulations, as shown in [29,30,31]. Such approach allows to investigate the effects of the PC design (volume, nozzle shape, hole diameter, hole shape, hole orientation and length) with proper reliability [32]. However, those analyses, due to their computational effort, usually cover one or few operating conditions of the engine. A more extended exploration of the engine behavior can be performed by 1D models, thanks to the lower computational burden. Reliable predictions can be achieved only if the 1D models are supplemented by proper phenomenological sub-models of in-cylinder phenomena.

In the light of the above considerations, in this work a quasi-dimensional model for a pre-chamber engine is employed to evaluate the combustion process and the pollutant emissions. The model aims at providing a description of all the basic phenomena occurring in an engine fitted with a PC, such as, turbulence evolution, turbulence jets, flame area enhancement, burn rate development, and pollutant formation.

According to the authors' knowledge, only a few predictive phenomenological models, trying to describe the basic physics behind a pre-chamber combustion system, are available in the current literature. In [33], the modelling is limited to the description of turbulence and heat transfer processes in the PC. In [34], the combustion in the main-chamber is described by imposed burn rate profiles (Wiebe-functions), without a direct phenomenological modeling of in-cylinder phenomena. A first attempt to handle the influence of combustion process in the pre-chamber towards the onset of the combustion in the main-chamber is described in [35]. Here, the burn rates in PC and MC are computed by Wiebe-functions, but combustion start and initial speed in the MC are controlled by the intensity of the turbulent jets ejected by the pre-chamber. Furtherly sophisticating the process description, Hiraoka et al. [36] assumed that the control of the initial phase of the MC combustion is driven by a conical turbulent jet released from the PC. Once jets end, the flame propagation is considered self-sustained, similarly to a conventional SI engine. In [37], the combustion development is described by an entrainment effect on the turbulent jets. They are assumed to entrain fresh charge, releasing subsequently heat. The increment of the flame front area was hypothesized in [38] due to jet penetration. A transition from a drop-shaped flame to hemispherical is assumed, as a function of a characteristic jet length. These last three approaches, even if including a physical description of the phenomena occurring in a PC engine, are characterized by a limited validation range, especially in terms of air/fuel ratio. Differently from the works above cited, the model here proposed is validated along a large range of relative air/fuel ratios (λ). As an additional original contribution, an unconventional multi-spherical propagation of the flame area in the MC is here adopted.

The present work deals with the experimental and numerical characterization of a Single Cylinder Engine (SCE)

equipped with an active pre-chamber. The paper is organized as follows. Firstly, the experimental set-up and 3D simulations, also employed for the phenomenological model validation, will be introduced. Then, the quasi-dimensional model will be presented, with emphasis on the combustion and pollutant descriptions. The model will be validated against experimental results in terms of overall performance, pressure traces, burning rates, combustion characteristics and pollutant emissions. 13 operating points at constant speed and load will be investigated, with the aim to underline engine performance and pollutant sensitivity to λ variations from stoichiometric up to ultra-lean operations (λ=1.0÷2.2).

Experimental Setup and Tests

Experimental setup - The experimental testing was conducted on a SCE at IFPEN facilities. This engine was designed within the EU H2020 EAGLE project. It is equipped with an active pre-chamber containing a spark-plug and a gasoline direct injector. The PC has 4 holes with two pairs of different hole size of around 1 mm diameter to exchange gases with the main combustion chamber. The details of the design process for this SCE have already been presented in [22].

The engine has a compression ratio of around 15:1 together with an early intake valve closing strategy (intake valve lift duration of 123 CAD). The intake and exhaust camshafts are phased in order to obtain maximum positive valve overlap. The fuel used for these tests is a standard E10 gasoline. The engine is operated with a gasoline port fuel injection at 200 bar. The same injection pressure is used for the gasoline direct injection inside the pre-chamber. The main engine specifications are listed in Table 1.

Pressurized intake air is provided by an external compressor through a sonic flowmeter in order to simulate boosted conditions at the test bench. The intake dry air is conditioned at 40 °C for all tests. An exhaust flap is used to simulate the backpressure of a real turbocharging system. For the tests reported here, the exhaust flap position is adjusted in order to set the exhaust pressure equal to the intake pressure. Oil and coolant are supplied by external electrically driven pumps and temperatures are kept constant at 90°C ± 2°C.

TABLE 1 Single cylinder engine main features.

Cylinder displacement		[cm^3]	408
Valves		[-]	4
Stroke		[mm]	90
Bore		[mm]	76
Compression ratio		[-]	~15:1
Fuel injection		[-]	gasoline port fuel injection, 200bar
Intake valve lift duration		[CAD]	123 @ 1 mm lift
EVC/IVO @ 1 mm lift		[CAD aTDC]	+14 / +3
Peak pressure capability		[bar]	180
Active PC	Volume	[cm^3]	~1
	Hole #	[-]	4, two pairs of different hole size
	Fuel inj.	[-]	gasoline direct injection, 200 bar
Start of injection MC		[CAD bTDC]	140
Start of injection PC		[CAD bTDC]	300

Ignition and injection timings are controlled with an in-house IFPEN control module. The global gasoline consumption is measured with a Low Pressure (LP) Coriolis Micromotion Elite CFM10 mass flowmeter located upstream the gasoline high pressure pump. A gasoline fuel rail distributes the fuel for the pre-chamber and for the main-chamber (port fuel injection). The gasoline mass flow rate injected in the PC is measured by a High Pressure (HP) Coriolis flowmeter. Therefore, the gasoline mass flow rate for port fuel injection can be obtained by subtracting the measure from the HP flowmeter to that from the LP flowmeter. Extremely low injection durations and fuel flow rates (<0.5mg/st) are used in the PC. This means that a shot-to-shot deviation can be expected for the intrinsic pre-chamber injector performance. In addition, even small rail pressure oscillations can further alter the shot-to-shot repeatability at such low fuel flow rates for which usual injection systems are not designed. Consequently, it means that the measure of the fuel mass flow rate injected in the PC might be inaccurate when extremely low. In the end, the consistency of each fuel mass flow rate is validated by the measure of LP Coriolis flowmeter.

Measurements of static pressures and temperatures are performed with conventional pressure transducers and thermocouples during an averaging interval of 30 seconds. The combustion process is monitored by different pressure transducers as follows:

- For the main combustion chamber, a Kistler 6043A pressure transducer is flush-mounted in the combustion chamber side roof;
- For the pre-chamber, a Kistler 6054 BR pressure transducer is flush-mounted in the PC volume;
- For the dynamic intake pressure, a Kulite XT123B190-100A pressure transducer is chosen and the signal is sampled by an Endevco charge amplifier;
- For the dynamic exhaust pressure, an AVL QC43D pressure sensor is implemented at the cylinder head outlet.

These pressure signals are recorded each 0.1 CAD for 300 consecutive engine cycles. Excepting the intake pressure sensor, all the others sensor signals have their sampling performed via Kistler 5064C22 charge amplifiers. The average pressure traces of both PC and MC pressure sensors are used for performing the heat release rate analyses, as detailed below. The pressure transducers in MC and PC are relative and both pressure signals are fitted by equalizing them with the average value of the high frequency exhaust pressure at the end of the exhaust stroke, close to Top Dead Center (TDC) when pressures at the exhaust and inside the cylinder are well balanced.

The main measurements performed on the single cylinder engine are summarized in Figure 1. Real time engine-out emissions (uHC, CH_4, CO, CO_2, O_2, NO and NO_2) are

FIGURE 1 Measurement schematic of the single cylinder engine at the test bed

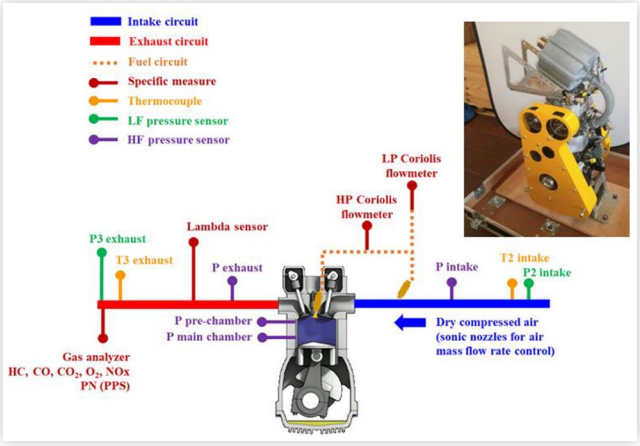

measured with Horiba MEXA-7100DEGR analyzer thanks to the exhaust gas sampling at the end of the exhaust line. The relative air/fuel ratio λ is determined based upon the exhaust gas composition. The principle is based on the balance of carbon, hydrogen, oxygen and nitrogen atoms between on the one side the exhaust gas molecules, and on the other side the air/fuel mixture at the intake. In these conditions, the reference λ is global, and it is not possible to determine the relative air/fuel ratios into the MC and PC separately. The experimental assessment of the relative air/fuel ratio into the pre-chamber is essential, but would require the use of advanced techniques (such as fast FID) with, however, significant implementation constraints due to the very limited access into the PC. This issue will be addressed with the help of the numerical analyses reported below.

Test specifications - The tests reported here are conducted in steady-state conditions at 3000 rpm engine speed and 13 bar IMEP. This operating point is selected based upon previous investigations as it is expected to be close to the sweet spot with maximal indicated efficiency. λ is the varied parameter. The fuel mass flow rate in the pre-chamber is optimized at λ = 1.67 and is kept constant at this optimal value for the whole λ variation. The spark advance is set for optimal combustion phasing (maximum torque), if there is no knocking limitation (in case of knock, delayed spark advances are used until the knock limit is achieved). Start of injection for main-chamber and pre-chamber are also optimized and set constant for the λ variation (see Table 1).

Indicated data post-processing - The indicated analysis is not straightforward in a PC engine because of the mass flow exchanged between main- and pre-chamber through the PC holes. On the other hand, the traditional rearranged energy balance equation employed for the extraction of the burn rate profiles relays on the hypothesis of constant mass [39]. To overcome this limitation, the post-processing of the pressure traces in both PC and MC is here realized by an inverse thermodynamic model developed by the authors, where the energy equation is coupled to the mass balance. The PC/MC mass exchange is computed based on isentropic nozzle flow equation, where the flow area is assumed equal to the geometrical area of the PC holes. This is multiplied by a discharge coefficient, which is tuned with the aim to reproduce the experimental PC/MC pressure difference during the compression phase. Preliminary calculations, not shown here for sake of brevity, highlighted that the proposed thermodynamic model and the conventional approach gave similar results for the burn rate estimation in the main-chamber. Concerning the PC, the thermodynamic model is the only path for the computation of the burn rate, where the hypothesis of constant mass is far from reality. It is worth underlining that all the indicated data discussed in the section about the results discussion, more specifically the experimental burn rate profiles, are derived by the thermodynamic model. Moreover, the latter is also employed for the extraction of characteristics combustion angles in PC and MC, when 10, 50 and 90% of mass fraction burned occur, labelled as MFB_{10}, MFB_{50}, and MFB_{90}, respectively. In the identification of the above combustion events, the burned mass is normalized by the current total mass, which in turn changes during time according to the PC/MC mass exchange.

CFD Simulation Setup

The present section describes the numerical setup used for the 3D simulation of the pre-chamber combustion system. 3D simulation has been carried out using commercial CFD code CONVERGE-2.4 [40]. The computational domain comprises of the intake and exhaust system and the simulation has been performed using the multi-cycle simulation approach. Therefore, the CFD results included in this work are derived from the second engine cycle.

The intake and exhaust boundary conditions in terms of pressure and temperature are obtained from the engine test bench results. The meshing of the computational domain has been carried out using the automated grid generation approach implemented in CONVERGE [41]. The base grid size in the computational domain is 2 mm which is refined up to 0.125 mm in order to appropriately capture the flow and combustion. Moreover, the main-chamber of the combustion system consists of a maximum grid size of 1 mm, while in the pre-chamber region the maximum grid size is 0.50 mm. The walls of PC and MC are refined up to 0.25 mm using the wall embedding feature in CONVERGE. Furthermore, the adaptive mesh refinement tool is used in order to perform local grid refinement in the zones of strong gradients of temperature and velocity fields.

Simulation time step has been managed using the variable time step approach which modifies the time step based on the maximum limit on Courant-Friedrichs- Lewy number. Gas simulation has been performed using the Redlich-Kwong equation of state. The RNG $k-\epsilon$ is used for the turbulence modeling with the standard law of wall approach [42]. Heat transfer between the gas and walls is modelled using O'Rourke and Amsden model [43].

For modelling of combustion, the extended coherent flame model [44,45] is used, which is based on the flame surface density approach. SI event in the pre-chamber is replicated using the imposed spark-ignition model [46] adapted for RANS calculations. In addition, the end gas auto-ignition

has been modelled with help of tabulated kinetics for ignition look-up table.

Engine Model Description

The experimental set-up is schematized in a 1D framework, implemented in a commercial software (GT-Power™). A 1D approach is hence followed for the description of flow within intake and exhaust pipes, while the in-cylinder phenomena are described by phenomenological sub-models, developed by the authors and implemented under the form of "user coding". The measured flow coefficients are imposed in the intake and exhaust valve objects. The average pressure/temperature measured signals are imposed in the simulations at the intake and exhaust environments. In this track, the experimental spark timing is imposed as an input. The injection process is simulated by standard injection objects, where the injection timing, instantaneous fuel rate and total injected mass per cycle are assigned for both indirect MC injection and PC direct injection. More specifically, the injected mass per cycle is estimated by flowmeter measurements. The spray formation and evaporation, and the fuel wall impingement are not directly modeled, and empirical evaporation rates are assigned within both the chambers to roughly account for the above phenomena. This simplification is expected to not substantially affect the presented results, since the PC injection occurs very early during the intake stroke, while the MC injection is indirect, and hence adequate fuel evaporation and homogenization presumably take place.

The main-chamber of the engine is simulated as a conventional variable 0D volume, while the pre-chamber is described by a constant volume. PC and MC are linked by an orifice, whose diameter is selected to realize the same overall cross-sectional area as the real PC holes. The discharge coefficient of the orifice is selected to fit the experimental PC/MC pressure difference during the compression phase. Mass and energy balance equations are solved in both volumes and a filling/emptying method is used to estimate the mass exchange between them.

Combustion model - The in-cylinder simulation is based on a two-zone (burned and unburned) assumption, where the combustion sub-model estimates the burned mass rate. This is here computed by a re-arranged "fractal" combustion model, developed by the authors in the last years [47]. The main difference concerns the handling of the mutual influence between combustion processes occurring in MC and PC.

The combustion speed, for a conventional SI engine, is enhanced by the turbulence, in turn mainly produced during the intake and compression strokes. In a pre-chamber engine, as described in [18], the presence of turbulent jets ejected from the PC additionally promotes and supports the MC combustion, especially during its early stage. This phenomenology is considered by computing the burn rate expression as the sum of two terms, Eq. (2).

$$\left(\frac{dm_b}{dt}\right)_{overall} = \left(\frac{dm_b}{dt}\right)_{fractal} + \left(\frac{dm_b}{dt}\right)_{jet} \tag{2}$$

The first term defines the burning rate occurring in a conventional engine, where a corrugated thin flame front, with a surface A_T, locally propagates at laminar speed, S_L:

$$\left(\frac{dm_b}{dt}\right)_{fractal} = \rho_u A_T S_L = \rho_u A_L S_L \frac{A_T}{A_L} \tag{3}$$

where ρ_u is the unburned gas density, A_L (A_T) the laminar (turbulent) flame area. The wrinkling factor A_T/A_L describes the intensity of the surface corrugations due to the flame/turbulence interaction. In accordance with the fractal theory applied to the flame front geometry [47], the wrinkling factor can be evaluated based on length scales of the maximum and minimum flame wrinkling, L_{max} and L_{min}, respectively, and on the fractal dimension D_3, Eq. (4).

$$\frac{A_T}{A_L} = \left(\frac{L_{\max}}{L_{\min}}\right)^{D_3-2} \tag{4}$$

To evaluate the fractal dimension, an empirical correlation is applied, depending on the turbulence intensity and laminar flame speed, as reported in [48]. To estimate the laminar flame speed, S_L, a correlation derived from 1D simulations of flame propagation in a gasoline/air mixture is utilized [49]. This correlation applies for both stoichiometric and ultra-lean mixtures (from λ= 0.58 up to 2.00), covering most of the operating conditions considered in this work. The fractal model actually applies for a fully developed and freely expanding turbulent flame. It is worth underlining that, at the combustion process beginning, when the turbulence eddies are not able to effectively wrinkle the flame surface, the above-mentioned description of the flame front propagation cannot be directly considered. Likewise, at the combustion completion, due to the flame front interaction with the combustion chamber walls, a burning rate slowdown occurs. Under these conditions, proper modifications of the model formulation are included, as detailed discussed in a previous work of the authors [50].

By following the hypothesis that the jets entrain fresh charge (air and fuel) and that the entrained mass progressively burns and releases heat, the burning rate contribution due to the turbulent jets (second term in Eq. (2)) is estimated. The heat release rate is assumed to be proportional to the difference between the current entrained mass (m_{entr}) and its burned portion ($m_{b,entr}$), and it is inversely proportional to a characteristic time scale τ, Eq. (5). The latter is computed as the ratio between the Taylor length scale, Λ_T, and the laminar flame speed, S_L, on the basis of the well-known eddy burn-up approach [51]. The current total entrained mass, m_{entr}, is computed integrating its time derivative, Eq. (6), in turn estimated applying the semiempirical correlation proposed in [36]. The aforesaid depends on the mass flow rate coming out of the PC, $\dot{m}_{jet}$, on a tuning constant c_{jet} and on the density ratio between PC and MC. Likewise, the burned entrained mass, $m_{b,entr}$, is computed by the integration of Eq. (5).

$$\left(\frac{dm_b}{dt}\right)_{jet} = \frac{dm_{b,entr}}{dt} = \frac{m_{entr} - m_{b,entr}}{\tau}; \tau = \frac{\Lambda_T}{S_L} \tag{5}$$

$$\frac{dm_{entr}}{dt} = c_{jet}\dot{m}_{jet}\sqrt{\frac{\rho_{PC}}{\rho_{MC}}} \tag{6}$$

FIGURE 2 Flame front schematizations in PC and MC.

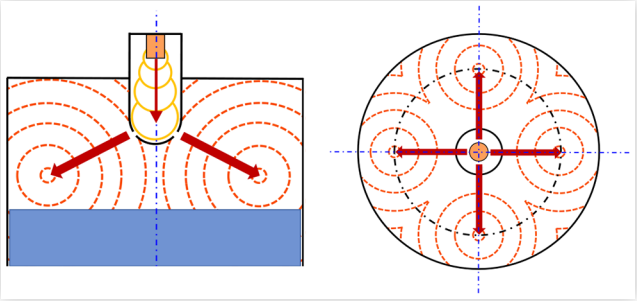

The combustion start in the PC is defined by the spark timing, given as a simulation input. On the contrary, the combustion onset in the MC is predicted according to the current flame radius in the PC. As soon as it exceeds a critical value, named r_{crit}, the MC combustion is activated. This parameter, normalized by the PC height, can be considered as an additional tuning constant, adjusting the combustion start in the MC. No direct estimation of the flame quenching through the PC holes is included in the model formulation. This phenomenology will be roughly considered by a proper selection of the tuning constants.

The laminar flame area A_L in Eq. (3) is calculated at each simulation step as a function of the burned gas volume and, in the MC case, also of the piston position. For the pre-chamber, a smooth spherically shaped propagation is assumed with a center moving at a speed proportional to the jet velocity. For the main-chamber, it is assumed that the flame mainly develops when the turbulent jets have almost dissipated their initial kinetic energy [53]. Presumed ignition sites are located along each turbulent jet, from which the flame propagates spherically. The position of sphere centers, unlike the PC, is assumed fixed during the combustion development, and given as an additional input parameter. Testing a moving center in the MC, it turns out that using this approach does not significantly improve the simulation accuracy, but considerably increases the computational time. In Figure 2 representative flame fronts are depicted to clarify the hypothesis about the flame front description above illustrated.

Combustion model tuning - For each chamber, the combustion model includes 3 tuning constants. They act respectively on the flame wrinkling, c_{wrk}, on the transition between an initially-laminar and a fully-turbulent combustion, c_{trans} as well as on the combustion tail, x_{wc}, [50]. The above constants, for a pre-chamber engine, can be set independently for both PC and MC. Furthermore, two additional tuning parameters are added to control the combustion transition between the two chambers. The first, r_{crit}, as stated above, triggers the MC combustion start, while the second, c_{jet}, acts on the burn rate enhancement depending on the penetration of the jets into the MC. Hence, the combustion model potentially includes 8 constants, but, as clarified below, one of them is not actually employed. A sequential methodology is followed for their identification:

1. The 3 tuning parameters are identified for the PC, following the procedure described in [50]. Briefly, a sequential identification of c_{trans}, c_{wrk} and x_{wc} is realized, searching for the better agreement between numerical and experimental combustion durations of early, main and completion phases, respectively.
2. c_{trans} for the MC is imposed equal to 0, under the hypothesis that the combustion begins in a fully turbulent stage. The values of r_{crit} and c_{jet} are selected with the aim of reproducing the combustion onset and burning speed in the main-chamber at the beginning of the process.
3. c_{wrk} and x_{wc} for the MC are selected to adjust the core of the combustion process and its completion according to the procedure in [50].

FIGURE 3 λMC (blue), λPC (red) and λF (green) inside the pre-chamber.

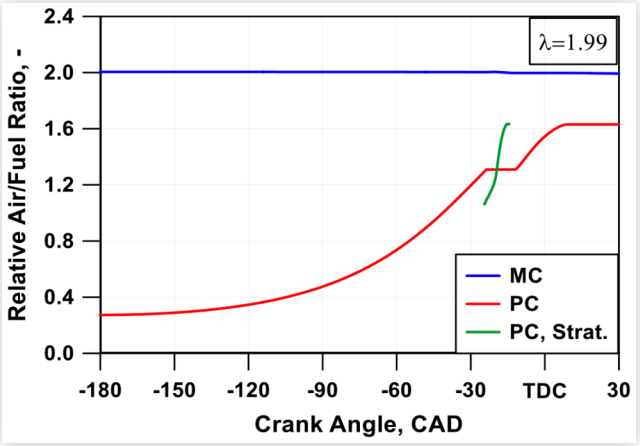

Resort to a trial-and-error procedure, a single set of tuning constants has been identified, determining the lowest average experiment/simulation error for all the investigated operating conditions, especially regarding the pressure cycles in both PC and MC.

PC mixture stratification and scavenging - A unique characteristic of the presented model is the possibility to account for mixture stratification in the PC. To explain this feature, Figure 3 shows the instantaneous predicted lambda levels in both pre- and main-chamber. At the end of the fuel injection inside the PC, a very rich mixture establishes ($\lambda_{PC} \approx 0.2 \div 0.3$). Later, all along the compression stroke, lean air/fuel mixture from the MC ($\lambda_{MC} \approx 1.8 \div 2.0$) is pushed through the PC holes, and the λ_{PC} rapidly increases on average. As confirmed by 3D CFD analyses, an incomplete mixing occurs in the pre-chamber, which exhibits a richer mixture close to the spark-plug and a leaner level, similar to one in the MC, at the holes [52]. To mimic such behavior, a simple correlation is here employed, which modifies the λ value at the flame borderline, λ_F, used to compute the laminar flame speed in the pre-chamber. The resulting λ_F profile is plotted in Figure 3, showing that it changes from a value richer than the average to a value leaner than the average, during the combustion evolution in the pre-chamber.

Another feature borrowed from the 3D analysis is the possibility to control the composition of the mass flow rate leaving the pre-chamber as soon as the pressure increases due to the combustion. Initially, unburned gases are mainly

FIGURE 4 Total (black), unburned (blue) and burned (red) mass flow rate contributions through the orifices (positive values mean the flow enters the pre-chamber).

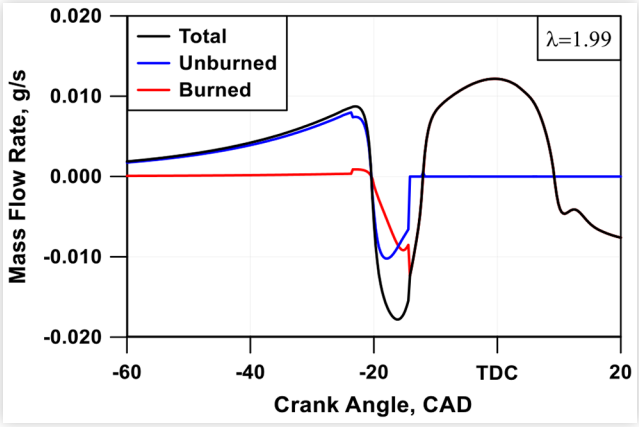

FIGURE 5 1D/3D comparison of turbulence intensity in PC and MC.

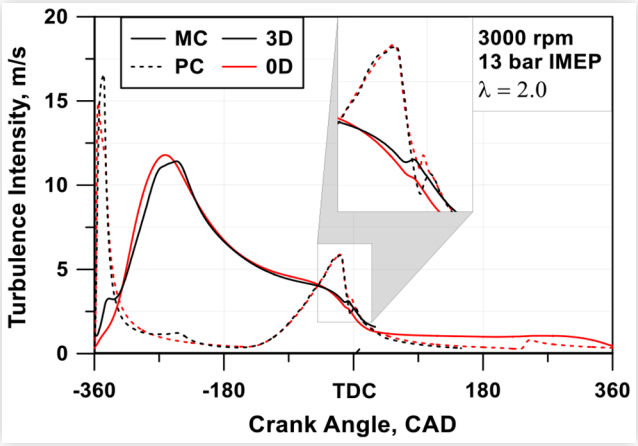

pushed away, while hot burned gases are ejected later during the pre-chamber combustion, mimicking a scavenging process in between a perfect displacement and a perfect mixing. The instantaneous total, unburned and burned mass flux contributions are depicted in Figure 4 in a representative case. The description of both PC mixture stratification and scavenging helps in correctly reproducing the burn rate and the pressure evolution in the pre-chamber. The combustion start in the main-chamber is also better triggered thanks to the above features.

Turbulence model - For the combustion model closure, the turbulence sub-model developed in [54] is used. This allows to estimate the levels of L_{max}, L_{min}, and u' in both the chambers. The sub-model belongs to the *K-k-T* family, and describes the energy cascade mechanism from the mean flow kinetic energy, *K*, to the turbulent one, *k*, also taking into account a balance equation for the tumble angular momentum, *T*. Additionally, it describes the turbulence production in the chambers, induced by the incoming/outcoming flow through the orifices [55]. An additional balance equation for the swirl motion is solved in the PC. The accuracy and the tuning procedure of the turbulence model for the considered PC engine was presented in a previous work of the authors [55].

Following a well-assessed hierarchical 0D-3D approach [54], the tuning constants of turbulence sub-model are selected in order to fit the 3D-derived turbulent intensity profiles in both chambers. Figure 5 shows a comparison between the turbulence intensity computed by the 0D model and the one resulting from the mass-averaged turbulence intensity field in the 3D model against the crank angle, for a representative operating condition. The agreement is very satisfactory for the MC (continuous red line) during the intake and compression phases, and also close to the firing TDC. Here, due to the collapse of the tumble motion, a less intense turbulence decay occurs. The PC turbulence (dashed red line) presents a turbulence peak close to the bottom dead center, which is due to the direct fuel injection. Then, it smoothly increases, during the compression stroke, as a consequence of the incoming flow from the main-chamber. The above trends are in good agreement with the 3D simulations. During the combustion phase, due to dissipative effects, a sudden turbulence decrease appears in the PC, discontinued by a local peak related to the flow coming from the main-chamber. This last appears in both 0D and 3D curves, although with a certain angular misalignment. The turbulence in MC exhibits a decreasing trend across the TDC similarly to the PC one, even if with a reduced rate. The dissipative effects determine a continuously decreasing tendency during the expansion stroke in both MC and PC, which are captured by the 0D model in good accordance with 3D results.

Heat transfer - A Woschni-like correlation is employed for the heat transfer in the pre- and main-chamber [56]. According to the standard formulation, the wall heat losses are assumed to be controlled by the pressure and temperature within the volume. An additional dependence on the mean flow velocity, derived by the above turbulence model, is introduced, which replaces the traditional dependence on the mean piston speed [56]. This allows to properly handle the heat transfer estimation within the PC, where the traditional Woschni correlation cannot be straightforwardly applied.

Pollutant emission - The model allows to estimate some regulated cylinder-out emissions, namely CO, uHC, and NO. For the evaluation of CO and NO, a multi-zone approach is applied in both PC and MC to mimic the burned gas temperature stratification. Each burned parcel is compressed/expanded adiabatically according to the in-cylinder pressure. The local zone temperatures are used to estimate the time evolution of the above pollutants according to chemical kinetics. More specifically, the well-known extended Zeldovich mechanism is applied for the evaluation of the NO kinetics [57], whereas the CO evolution is computed with a two-step reaction scheme [16]. The experimental findings show that in ultra-lean engines, the nitric emissions are mainly composed of NO_2. For this reason, in the adopted approach, the NO production derived by the Zeldovich mechanism is assumed to completely oxidize into NO_2 when the burned gases evolve along the exhaust pipes. Concerning the uHC simulation, the model is applied only in the MC, neglecting the PC contribution. The model considers uHC emissions related to both crevices and wall quenching. A simple filling and emptying model is applied for the estimation of uHC emission from the

crevice regions [58]. For the sake of simplicity, the only crevice region here considered is the volume between the cylinder liner and the top land of the piston ring pack. In this track, the temperature of the unburned gas trapped in this volume is considered to be the same as the piston wall. The pressure within the crevice is supposed equal to the cylinder one. Concerning wall quenching uHC source, a simplified model is here employed, where the wall flame extinction distance is estimated by the correlation in [59]. The area swept by the flame front is computed in real time during the simulation by a simplified geometrical schematization of the flame front. In this way, the amount of fresh gases which does not burn due to the flame propagation is appraised. The model, in the current version, does not consider the uHC formation from bulk flame quenching [60]. This phenomenon mainly depends on fuel inhomogeneities, which may cause the flame extinguishment in the combustion chamber regions where the mixture is the leanest. This is a complex 3D problem, which will be addressed in the next development of the model thorough the introduction of a presumed air/fuel stratification in the MC, possibly derived from 3D analyses.

UHCs from crevices and wall quenching partly oxidize according to the kinetic rate proposed in [61]. It is worth underlying that the uHC model interacts with the calculation of the burn rate, since the uHC trapped in the crevices and subjected to the wall quenching do not participate to the heat release due to the regular combustion development. Only the fraction of above contributions which post-oxidizes is taken into account in the calculation of the burn rate. A tunable fraction (7% in the results proposed in the following) of post-oxidized HC is assumed to not fully oxidize and to transform in CO, which is added to the CO production from the above-mentioned two-step kinetic mechanism. This last would have resulted in a negligible CO formation due to the ultra-lean operation, typical of the considered engine. Hence, the HC post-oxidation is assumed to be the main responsible for CO emission. The estimated instantaneous concentrations of the pollutant emissions are imposed as boundary conditions at the exhaust pipe inlet. In this way, the species are transported along the exhaust line, and pollutants are detected at the same location where the probes for pollutant measurement are placed. The pollutant emissions are provided as output under the form of both concentrations and Indicated Specific (IS) indices, namely $ISNO_2$, ISuHC and ISCO.

Engine Model Validation

The model validation is realized by comparing the simulation predictions with the experimental findings for all the available operating points. In a first stage, it is discussed in terms of experimental/numerical comparisons between global performance as a function of the total relative air/fuel ratio, including the Root Mean Squared Error (RMSE) as a global indicator of the model accuracy. The air flow rate, depicted in Figure 6, is satisfactorily predicted, with an error within the band ± 1%. The related RMSE of 0.39 kg/h denotes an accurate schematization of the intake and exhaust pipe geometry and a proper specification of the valve flow coefficients. The IMEP values,

FIGURE 6 Experimental/numerical air flow rate comparison against the relative air/fuel ratio.

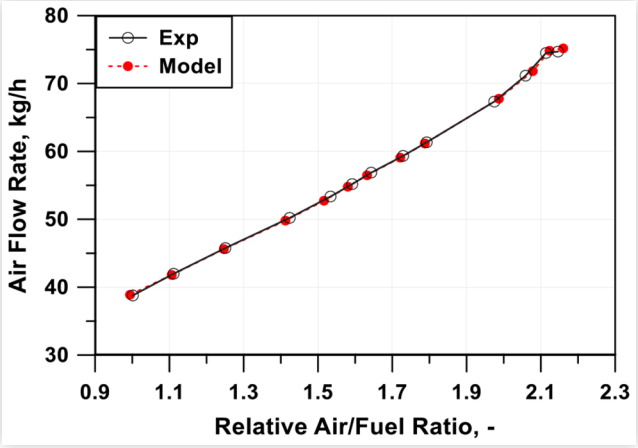

FIGURE 7 Experimental/numerical IMEP comparison against the relative air/fuel ratio, experimental CoV of IMEP.

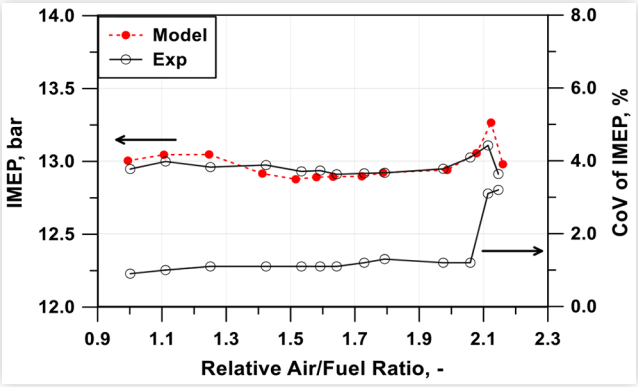

illustrated in Figure 7, are satisfactorily computed, with a model error of ± 1% in most of the operating points, and a RMSE of 0.062 bar. Figure 7 also depicts the measured Coefficient of Variation (CoV) of IMEP. This highlights an allowable level (below 1.3%) for λ lower than 2, while substantially increases for the leanest cases. These additional data will help the interpretation of the emissions results. The combination of IMEP and air flow rate results in a good prediction of the indicated efficiency, as shown in Figure 8. The model finds a maximum efficiency of about 47% at $\lambda = 2$, in accordance with the experimental findings, with an improvement greater than 5 points compared to the stoichiometric case. Moving from the stoichiometric case, leaning the mixture determines less intense heat losses and more favorable thermo-chemical properties of the in-cylinder mixture (lower ratio of specific heats), reflecting on the efficiency improvement. The more pronounced efficiency gaining for λ lower than 1.5 is promoted by the possibility of progressively anticipating the combustion phasing, thanks to a higher knock resistance of the air/fuel mixture, as clarified in the following. Moving towards λ greater than 2, the efficiency reduction is caused by the combustion slowdown, which also determines a greater presence of uHC, which subtracts a fraction of heat to the combustion process. Also, this aspect will be discussed below,

FIGURE 8 Experimental/numerical indicated efficiency comparison against the relative air/fuel ratio.

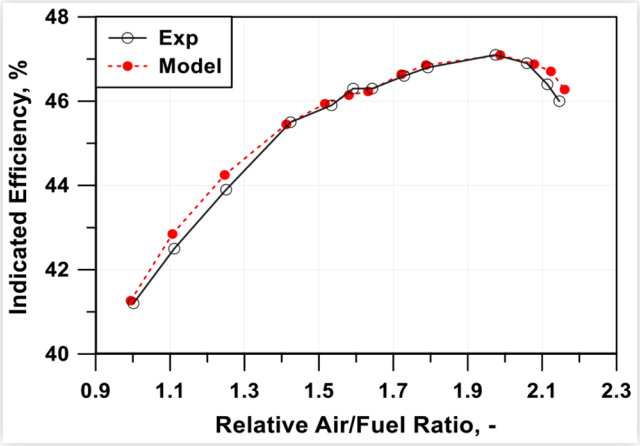

FIGURE 9 Numerical wall heat losses normalized by the total fuel energy in PC and MC against the relative air/fuel ratio.

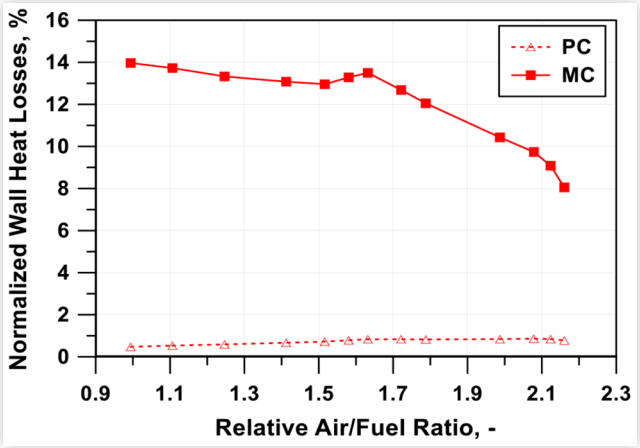

in the comments to the pollutant emission model results. The interpretation of the efficiency variation with λ is supported by Figure 9, which depicts the computed wall heat losses. More specifically, the figure shows the wall heat losses in PC and MC, normalized by total energy introduced in the engine by the injected fuel. Figure 9 points out a relative reduction of the wall heat losses by leaning the air/fuel mixture, which is due to reducing in-cylinder temperatures. In particular, the losses pass from about 14% under stoichiometric mixture down to about 8% for the leanest case. The simulations also highlight that the wall heat losses in the pre-chamber have a lesser importance compared to the MC ones, and slightly increases with λ.

Since the spark timing is imposed in simulations, the MFB_{50} angular position in PC and MC can be considered as a measure of the overall combustion model reliability. Note that the MFB_{50} angular position extracted from the 1D simulation is computed as the ratio of the burned mass and the current total mass, accounting for the PC/MC mass exchange, congruently with the approach used in the indicated analysis. Figure 10 shows a good model accuracy for both pre-chamber and main-chamber, with an RMSE of 1.44 CAD and 0.44

FIGURE 10 Experimental/numerical *MFB50* comparison in PC and MC against the relative air/fuel ratio.

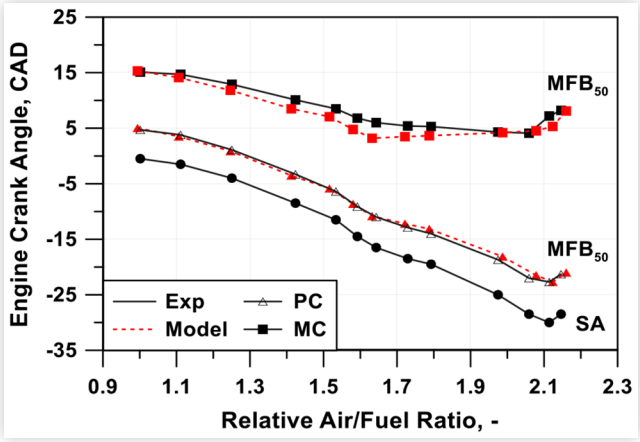

CAD, respectively. The figure confirms that, leaning the mixture, the spark event can be progressively advanced thanks to the higher knock resistance of the in-cylinder mixture. The plot also underlines that an experiment-advised optimal MFB_{50} at about 5 CAD aTDC is reached when λ is greater than 1.5, while, for lower λ, a delayed non-optimal combustion phasing is mandatory. Figure 10 also highlights that the combustion speed in the PC is slightly sensitive to the overall air/fuel, being the MFB_{50} angular position primarily controlled by the SA phasing. This is due to the flexibility of an active pre-chamber device, where the PC local air/fuel ratio can remain close to the stoichiometric level whatever is the λ in the main-chamber. This is clearly shown in Figure 11, where the estimated λ level in the pre-chamber at the spark event is plotted against the total air/fuel ratio. Figure 10 also points out that the combustion speed in the MC slows down by leaning the reactive mixture. This is well captured by the model, thanks to the reduction of the laminar flame speed.

A satisfactory prediction of the combustion phasing and speed in both PC and MC is confirmed by the comparisons of the peak pressure crank angle locations and levels, depicted in Figure 12 and Figure 13, respectively. Concerning the MC,

FIGURE 11 Numerical relative air/fuel ratio in the pre-chamber at the spark event against the relative air/fuel ratio.

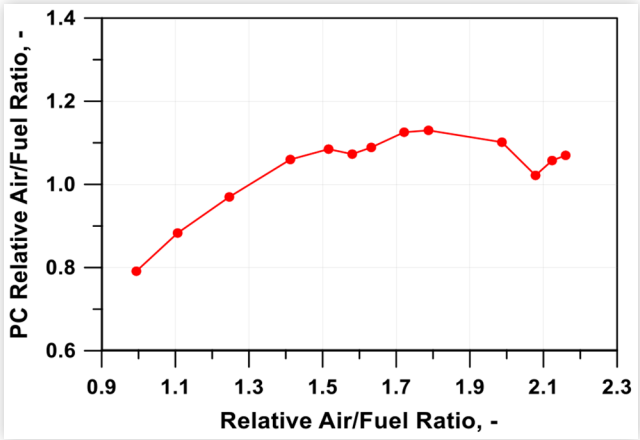

FIGURE 12 Experimental/numerical angular position comparison of peak pressure in PC and MC against the relative air/fuel ratio.

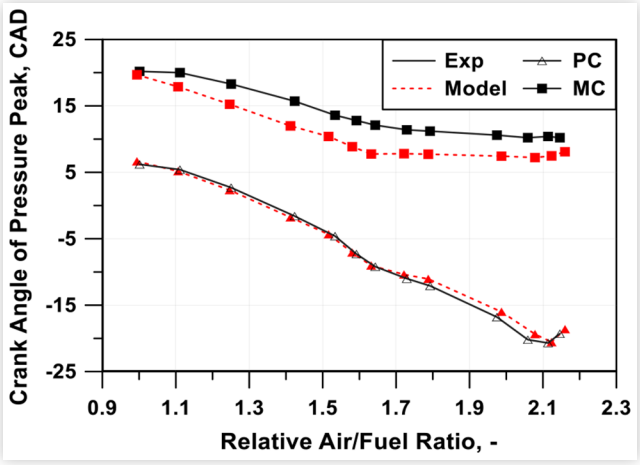

FIGURE 13 Experimental/numerical comparison of peak pressure in PC and MC against the relative air/fuel ratio.

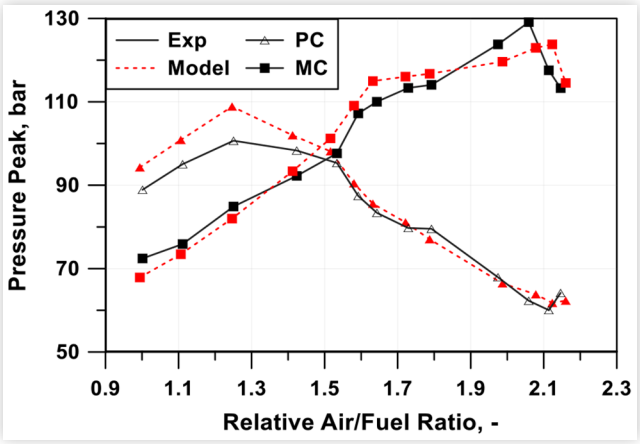

the predicted peak pressure angular position appears slightly advanced in the comparison with the experimental counterpart. This is due to some inaccuracies in the description of the combustion tail, as better clarified in the following. The results in terms of global performance parameters and combustion events demonstrate the consistency and reliability of the proposed numerical approach, considering the relevant variation range of the air/fuel ratio and the absence of a case-dependent model tuning.

A deeper insight in the combustion model reliability is given by the experimental / numerical comparisons of the pressure traces (Figure 14) for 4 representative cases, and of the related burn rates (Figure 15). In those figures the experimental (numerical) data are represented with black (red) curves, continuous or dashed for the MC or PC, respectively. As a first consideration, the pressure difference between PC and MC during the compression phase is well captured by the simulation, thanks to a proper selection of the flow coefficient of the orifice linking PC and MC. The pressure rises in the PC due to the combustion is well reproduced in all case. Minor

FIGURE 14 Experimental/numerical comparison of MC and PC pressure traces at (a) λ=1.00, (b) λ=1.54, (c) λ=1.99, (d) λ=2.18.

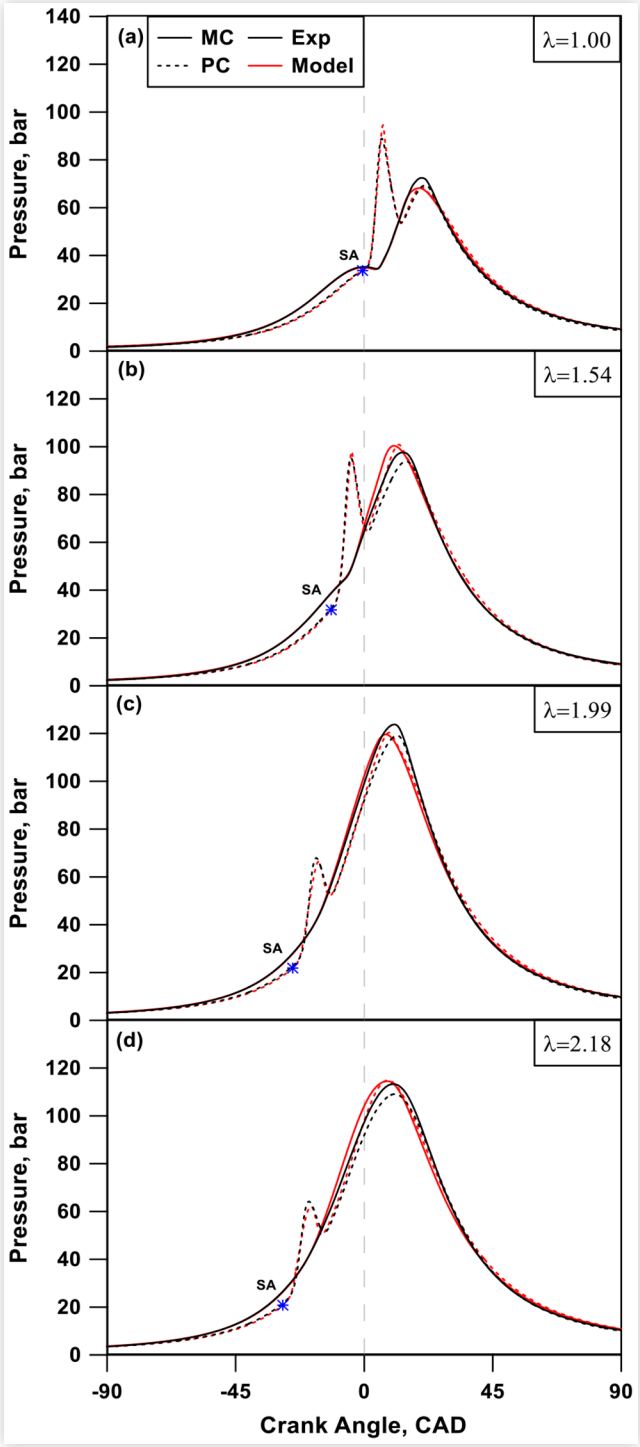

inaccuracies appear in the pressure decreasing phase, especially for the leaner cases. Concerning the MC, the model accuracy in the first part of the combustion process is very good. More specifically, the simulation demonstrates to adequately predict the burn rate knee, which is due to the combustion enhancement caused by the hot turbulent jets ejected by the PC.

FIGURE 15 Experimental/numerical comparison of MC and PC burn rates at (a) λ=1.00, (b) λ=1.54, (c) λ=1.99, (d) λ=2.18.

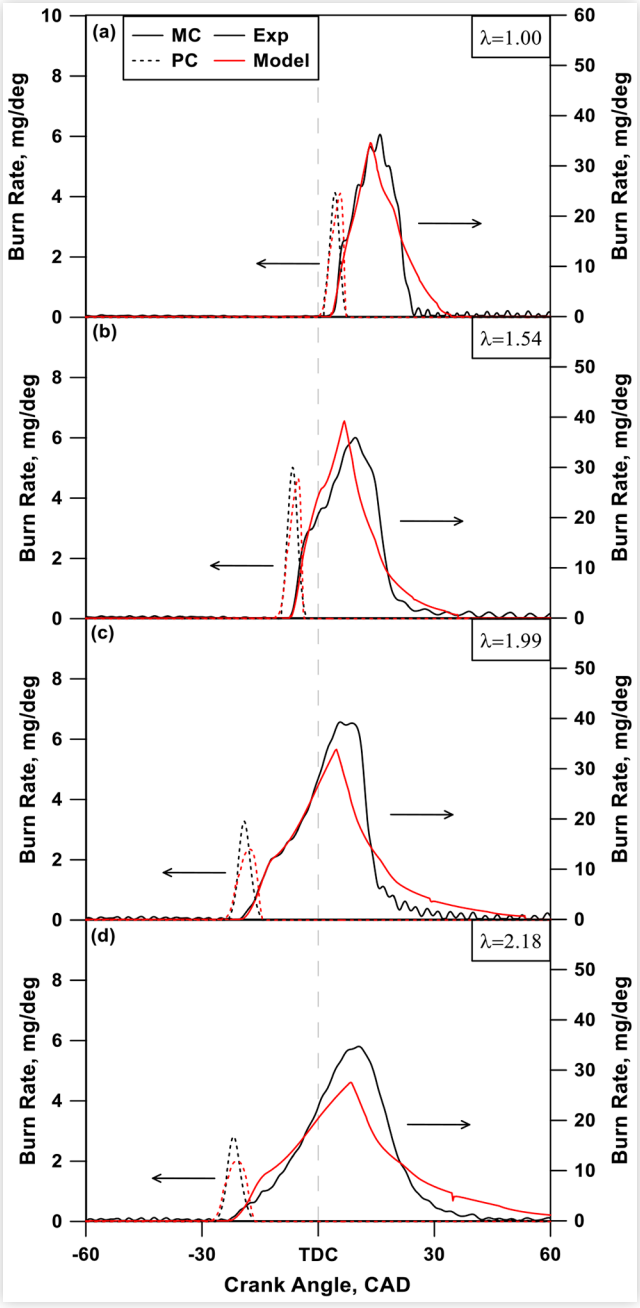

FIGURE 16 Experimental/numerical $ISNO_2$ comparison against the relative air/fuel ratio.

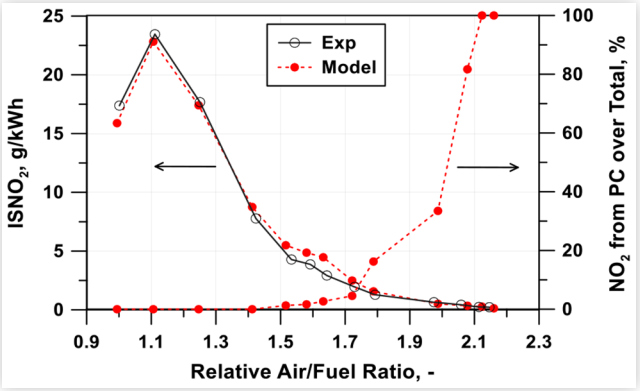

The model follows quite well the λ variation, overestimating its effect only for the leanest case (Figure 14(d)). Moving on during the combustion, the burn rate presents a slope reduction, which can be related to the onset of a regular self-sustained flame propagation. This rate reduction is more evident in the cases with leaner air/fuel mixtures, and this is captured by the model by the reduction of the laminar flame speed. After this phase, the burn rate presents its maximum, followed by a gradual decrease, caused by the contact of the flame front with the combustion chamber walls and by the cross-interaction of the multiple flame fronts. The systematic disagreement between numerical and experimental trends towards the combustion end is probably due to the absence in the flame front geometrical schematization of its conical propagation. This possibly sustains the flame front surface extension during the last portion of the process, but, at the combustion completion, this also determines its sudden decrease.

As an additional results of the proposed methodology, in Figure 16-Figure 18, the experimental/numerical comparisons between the indicated specific NO_2, uHC and CO emissions are reported. Figure 16 underlines a good model accuracy in the prediction of NO_2 emissions. As expected, while leaning the air/fuel mixture, thanks to the lower temperatures of the burned gas, the NO_2 production rate is less intense. As a peculiar feature of the proposed approach, the model allows to distinguish the NO_2 productions from PC and MC, as reported in Figure 16. This last depicts the percentage of NO_2 arising from the PC, normalized by the total production. Figure 16 points out that the main source of NO_2 is the main-chamber for λ below 1.7, while leaning the mixture the PC production assumes an increasing importance, and becomes the unique contribution for λ above 2.1. In Figure 17, both computed and measured uHC emission present an increasing trend when the mixture becomes leaner. This can be justified by a less effective post-oxidation process of the uHC released from the crevice volumes, due to lower in-cylinder temperatures. The model is able to describe the above phenomenology, denoting a sensitivity to λ variations similar to the experimental data. On the other hand, excepting for the less lean cases, it underestimates the ISuHC level. For the leanest cases (λ>2), the measured ISuHC presents a higher sensitivity to λ, whose trend brings up. This is probably due to the combined effect of combustion cyclic instabilities (see Figure 7), which determines the combustion incompleteness of some individual cycles in experiments, and to the increase of the relative weight of the uHC related to flame quenching. While the first effect cannot be straightforwardly taken into account in the proposed methodology, which does not consider the cyclic variability, the second effect is partly modeled. The relevance of such aspect is highlighted in Figure 17, where an additional line is introduced, depicting the numerical results without uHC related to wall quenching. A better prediction would have been expected if, in addition to wall quenching, the bulk quenching had been taken into account. This issue will

FIGURE 17 Experimental/numerical ISuHC comparison against the relative air/fuel ratio.

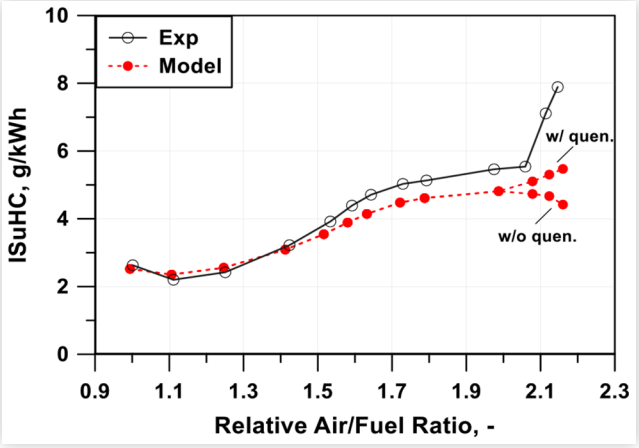

FIGURE 18 Experimental/numerical ISCO comparison against the relative air/fuel ratio.

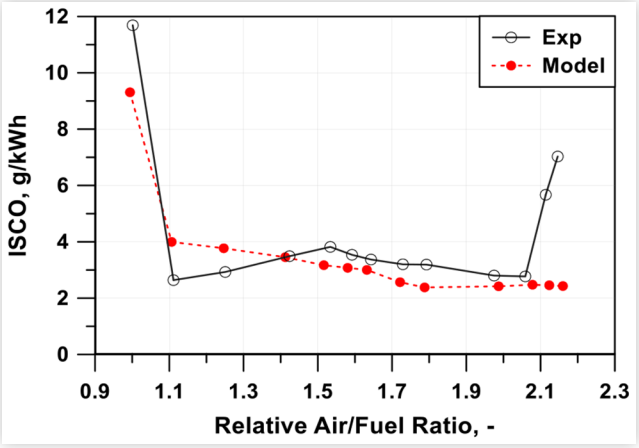

be addressed in the next development of this activity. As already mentioned, the progressive increase of the uHC emission is one of the reasons of the indicated efficiency trend flattening and reduction by leaning the mixture. This is satisfactorily captured by the model, as highlighted in Figure 8. Figure 18 reports the experimental/numerical results for ISCO. The figure shows a reduced sensitivity of experimental ISCO to the λ variation, excepting for the extreme cases. The operating point at nominal stoichiometric air/fuel mixture features a predicted λ slightly lower than the unit. In this condition, even a small O_2 deficit causes, as known, a certain CO over-production, if compared to lean cases. This is detected by the model, even if with a reduced extent in the comparison with experimental datum. For the leanest cases (λ>2), as already mentioned, incomplete combustions and flame bulk quenching may occur in some individual cycles, affecting CO production. Those aspects are not yet considered in the presented model and constitute potential improvements for the next developments. In the operations with intermediate λ values, predicted CO emission presents an almost flat trend with the air/fuel mixture, similarly to the experimental counterpart. This behavior is captured mainly thanks to the CO contribution arising from HC post-oxidation. Despite of the above-mentioned inaccuracies, the pollutant production sub-model furnishes satisfactory results, being capable to correctly sense the superimposed variations of in-cylinder thermodynamic conditions (pressure, temperature) and composition (air/fuel mixture).

As a final consideration, it worth mentioning that the model potential was also tested at engine speeds and loads different from the operating point here considered. The related results are not shown here for sake of brevity. In those analyses, a combustion lengthening emerged under ultra-lean conditions (λ = 2.0) at increasing speed. Indeed, in these conditions, the laminar flame speed is rather reduced over the whole operating domain, and the combustion speed enhancement due to turbulence increase at rising speed is not enough to avoid or limit the combustion angular duration lengthening. The engine load instead seems to not particularly affect combustion duration, leading to an unallowable lengthening only at very low load. This is due to a less effective PC scavenging and to undesired enrichment of PC air/fuel mixture. Those outcomes will be experimentally verified in the next development of this activity.

Conclusions

In this work, the potentialities of an ultra-lean pre-chamber SI engine, developed in the framework of the EU H2020 EAGLE project, are presented through numerical and experimental analyses. For this work, the single cylinder engine under study was tested in a representative operating condition (3000 rpm at 13 bar IMEP) over a λ sweep from stoichiometric up to ultra-lean (λ = 2.2) conditions.

A 1D model of the tested engine was developed, including refined phenomenological sub-models describing complex in-cylinder phenomena, such as turbulence, combustion, heat transfer, and pollutant emissions. The fractal combustion model, suitable for a conventional SI engine, was extended to handle the pre-chamber architecture. The model takes into account the turbulence and burn rate enhancements in the main-chamber due to the burned gas jets emerging from the pre-chamber.

Both numerical and experimental results demonstrated the potential of this combustion concept, highlighted by an improvement of the indicated efficiency greater than 5 points passing from stoichiometric to ultra-lean conditions, with a maximum at λ = 2.0.

The model accuracy was verified against the experimental pressure traces in both PC and MC and against the global engine performance parameters. The results underlined the good model capability in predicting air flow rate, IMEP and indicated efficiency. Concerning the pressure traces, the related burn rate profiles and the main combustion events, the experimental / numerical agreement is satisfactory, considering that the results were obtained without modifying the tuning constants for all the tested operating conditions. The combustion completion description denoted some inaccuracies, probably due to some lack in the description of the flame front surface in this combustion phase. The model also

proved a good prediction of NOx emissions, while uHC and CO computations denoted a lower accuracy.

Next steps of the numerical activity will concern the modeling of the flame quenching effects that occur when the flame passes though the PC holes or when the turbulence-induced strain rate becomes very high. The simulation of the flame bulk quenching will be introduced, as well, to improve uHC model predictivity under very lean conditions ($\lambda > 2.0$). Moreover, a refined description of the flame front geometry will be introduced, also considering the possibility of a conical flame propagation, in addition to the already considered spherical propagation.

Contact information

V. De Bellis, Researcher,
vincenzo.debellis@unina.it

E. Malfi, PhD Candidate,
enrica.malfi@unina.it

F. Bozza, Full Professor,
fabio.bozza@unina.it
University of Naples "Federico II",
Naples, Italy,
+39-081-7683264.

D. Kumar, Research and Innovation Engineer,
brt.deepak@gmail.com

D. Serrano, Research and Innovation Engineer,
david.serrano@ifpen.fr

A. Dulbecco, Research and Innovation Engineer,
alessio.dulbecco@ifpen.fr

J.M. Zaccardi, Project Leader,
jean-marc.zaccardi@ifpen.fr
IFP Energies nouvelles, Institut Carnot IFPEN TE,
+33 (0)4 37 70 20 63.

References

1. Zaccardi, J.M. and Brandstätter, B., "Research needs on Energy, Powertrains, and Electrification," EARPA Position Paper, 2020, https://www.earpa.eu/ENGINE/FILES/EARPA/INTRANET/UPLOAD/POSITION_PAPERS/position_paper_Energy%20Powertrains%20And%20Electrification.pdf, accessed 27 October 2020.
2. International Energy Agency, Energy Technology Perspectives 2012: Pathways to a Clean Energy System, 2012, doi:10.1787/20792603.
3. Brossard, J.L., "The Energy Mix and Its Impact on Multiple Automotive Topics," in *SIA Powertrain Conference*, 2018.
4. Subramanian, V., Gillet, R., and De Paola, G. "Future Evolutions of Diesel Engine Technology and its Powertrain Trends Influencing CO_2 Emissions in Europe," in *SIA Powertrain Conference*, 2018.
5. De Bellis, V., Bozza, F., Siano, D., and Gimelli, A., "Fuel Consumption Optimization and Noise Reduction in a Spark-ignition Turbocharged VVA Engine," *SAE International Journal of Engines* 6(2):1262-1274, 2013, doi:10.4271/2013-01-1625.
6. Roberts, M., "Benefits and Challenges of Variable Compression Ratio (VCR)," SAE Technical Paper 2003-01-0398, 2003, http://dx.doi.org/10.4271/2003-01-0398.
7. Francqueville, L., and Michel, J., "On the Effects of EGR on Spark-Ignited Gasoline Combustion at High Load," *SAE Int J Engines* 7(4):1808-1823, 2014, doi:10.4271/2014-01-2628.
8. Hoppe, F., Thewes, M., Baumgarten, H., and Dohmen, J., "Water Injection for Gasoline Engines: Potentials, Challenges, and Solutions," *International J of Engine Research* 17(1):86-96, 2016, doi:10.1177/1468087415599867.
9. Sens, M., Günther, M., Medicke, M., and Walther, U., "Developing a Spark-Ignition Engine with 45% Efficiency," *MTZ worldwide* 81:46-51, 2020, doi:10.1007/s38313-020-0194-x.
10. Splitter, D., Boronat, V., Chuahy, F. and Storey, J., "Performance of Direct Injected Propane and Gasoline in a High Stroke-to-Bore Ratio SI Engine: Pathways to Diesel Efficiency Parity with Ultra Low Soot," in *THIESEL Conference*, 2020.
11. Bozza, F., De Bellis, V., Teodosio, L., Tufano, D., and Malfi, E., "Techniques for CO2 Emission Reduction over a WLTC. A Numerical Comparison of Increased Compression Ratio, Cooled EGR and Water Injection," SAE Technical Paper 2018-37-0008, 2018, http://dx.doi.org/10.4271/2018-37-0008.
12. Iida, N., "Research and Development of Super-Lean Burn for High Efficiency SI Engine. Challenge for Innovative Combustion Technology to achieve 50% Thermal Efficiency," in *9th Conference on Modeling and Diagnostics for Advanced Engine Systems (COMODIA)*, 2017, doi:10.1299/jmsesdm.2017.9.PL-1.
13. Ratnak, S., Kusaka, J., Daisho, Y., Yoshimura, K. et al., "Experiments and Simulations of a Lean-Boost Spark Ignition Engine for Thermal Efficiency Improvement," *SAE Int. J. Engines* 9(1):379-396, 2016.
14. Germane, G., Wood, C., and Hess, C., "Lean Combustion in Spark-Ignited Internal Combustion Engines - A Review," SAE Technical Paper 831694, 1983, http://dx.doi.org/10.4271/831694.
15. Rapp, V., Killingsworth, N., Therkelsen, P. et al., *Lean Combustion* 2nd Edition (London: Lean-Burn Internal Combustion Engines, 2016), 111-146, doi:10.1016/C2013-0-13446-0.
16. Heywood, J.B., *Internal Combustion Engine Fundamentals*. Vol. 930 (New York: Mcgraw-Hill, 1988). ISBN:007028637X.
17. Moriyoshi, Y., Kuboyama, T., Kaneko, M., Yamada, T., and Sato, H., "Fuel Stratification Using Twin-Tumble Intake Flows to Extend Lean Limit in Super-Lean Gasoline Combustion," SAE Technical Paper 2018-01-1664, 2018, http://dx.doi.org/10.4271/2018-01-1664.
18. Mueller, C., Morcinkowski, B., Habermann, K., Uhlmann, T. and Schernus, C., "Development of a Pre-chamber for Spark Ignition Engines in Vehicle Applications," in *4th International Conference on Ignition Systems for Gasoline Engines*, Dec. 2018, doi:10.5445/IR/1000088588.
19. Jung, D., Sasaki, K., Sugata, K., Matsuda, M. et al., "Combined Effects of Spark Discharge Pattern and Tumble

Level on Cycle-to-Cycle Variations of Combustion at Lean Limits of SI Engine Operation," SAE Technical Paper 2017-01-0677, 2017, http://dx.doi.org/10.4271/2017-01-0677.

20. Luszcz, P., Takeuchi, K., Pfeilmaier, P., Gerhardt, M., et al, "Homogeneous Lean Burn Engine Combustion System Development Concept Study," in *18th Stuttgart International Symposium*, 2018, doi:10.1007/978-3-658-21194-3_19.
21. Mazda Next-generation Technology, Skyactiv-X Next-Generation Gasoline Engine, press information, October 2017, https://insidemazda.mazdausa.com/press-release/mazda-next-generation-technology-press-information/, accessed 27 October 2020.
22. Serrano, D., Zaccardi, J., Müller, C., Libert, C. et al., "Ultra-Lean Pre-Chamber Gasoline Engine for Future Hybrid Powertrains," *SAE Int. J. Adv. & Curr. Prac. in Mobility* 2(2):607-622, 2020, doi:10.4271/2019-24-0104.
23. Sens, M., Binder, E., Reinicke, P.-B., Riess, M., Stappenbeck, T. and Wöbke, M., "Pre-Chamber Ignition and Promising Complementary Technologies," in *27th Aachen Colloquium Automobile and Engine Technology*, 2018.
24. Attard, W., Fraser, N., Parsons, P., and Toulson, E., "A Turbulent Jet Ignition Pre-chamber Combustion System for Large Fuel Economy Improvements in a Modern Vehicle Powertrain," *SAE International Journal of Engines* 3(2):20-37, 2010, www.jstor.org/stable/26275544.
25. Jamrozik, A., "Lean Combustion by a Pre-chamber Charge Stratification in a Stationary Spark Ignited Engine," *Journal of Mechanical Science and Technology* 29(5):2269-2278, 2015, doi:10.1007/s12206-015-0145-7.
26. Toulson, E., Schock, H., and Attard, W., "A Review of Pre-Chamber Initiated Jet Ignition Combustion Systems," SAE Technical Paper 2010-01-2263, 2010, http://dx.doi.org/10.4271/2010-01-2263.
27. Lumsden, G., and Watson, H., "Optimum Control of an S.I. Engine with a λ=5 Capability," SAE Technical Paper 950689, 1995, http://dx.doi.org/10.4271/950689.
28. Schumacher, M., and Wensing, M., "A Gasoline Fuelled Pre-Chamber Ignition System for Homogeneous Lean Combustion Processes," SAE Technical Paper 2016-01-2176, 2016, http://dx.doi.org/10.4271/2016-01-2176.
29. Jamrozik, A., Tutak, W., Kociszewski, A., and Sosnowski, M., "Numerical Simulation of Two-stage Combustion in SI Engine with Prechamber," *Applied Mathematical Modelling* 37(5):2961-2982, 2013, doi:10.1016/j.apm.2012.07.040.
30. Shah, A., Tunestål, P., and Johansson, B., "CFD Simulations of Pre-Chamber Jets' Mixing Characteristics in a Heavy Duty Natural Gas Engine," SAE Technical Paper 2015-01-1890, 2015, http://dx.doi.org/10.4271/2015-01-1890.
31. Gentz, G., Thelen, B., Litke, P., Hoke, J., and Toulson, E., "Combustion Visualization, Performance, and CFD Modeling of a Pre-Chamber Turbulent Jet Ignition System in a Rapid Compression Machine," *SAE International Journal of Engines* 8(2):538-546, 2015, doi:10.4271/2015-01-0779.
32. Biswas, S., and Qiao, L., "A Numerical Investigation of Ignition of Ultra-Lean Premixed H_2/Air Mixtures by Pre-Chamber Supersonic Hot Jet," *SAE Int. J. Engines* 10(5):2231-2247, 2017, doi:10.4271/2017-01-9284.
33. Bardis, K., Xu, G., Kyrtatos, P., Wright, Y.M. et al., "A Zero Dimensional Turbulence and Heat Transfer Phenomenological Model for Pre-Chamber Gas Engines," SAE Technical Paper 2018-01-1453, 2018, http://dx.doi.org/10.4271/2018-01-1453.
34. Benajes, J., Novella, R., Gomez-Soriano, J., Martinez-Hernandiz, P.J. et al., "Evaluation of the Passive Pre-chamber Ignition Concept for Future High Compression Ratio Turbocharged Spark-ignition Engines," *Applied Energy* 248:576-588, 2019, doi:10.1016/j.apenergy.2019.04.131.
35. Tolou, S., and Schock, H., "Experiments and Modeling of a Dual-mode, Turbulent Jet Ignition Engine," *International Journal of Engine Research* 21(6):966-986, 2020, doi:10.1177/1468087419875880.
36. Hiraoka, K., Nomura, K., Yuuki, A., Oda, Y. et al., "Phenomenological 0-Dimensional Combustion Model for Spark-Ignition Natural Gas Engine Equipped with Pre-Chamber," SAE Technical Paper 2016-01-0556, 2016, http://dx.doi.org/10.4271/2016-01-0556.
37. Shojaeefard, M.H., and Keshavarz, M., "Flame Propagation Model for a Rotary Atkinson Cycle SI Engine," *International Journal of Automotive Technology* 19(1):9-25, 2018, doi:10.1007/s12239-018-0002-7.
38. Auer, M., and Wachtmeister, G., "Phenomenological Models for Pre-Calculation of the Combustion in Gas Engines," *MTZ worldwide* 70(6):52-59, 2019, doi:10.1007/BF03226962.
39. Cheung, H., and Heywood, J., "Evaluation of a One-Zone Burn-Rate Analysis Procedure Using Production SI Engine Pressure Data," SAE Technical Paper 932749, 1993, https://doi.org/10.4271/932749.
40. Converge v2.4 Manual, Convergent Science, 2017.
41. Senecal, P., Richards, K., Pomraning, E., Yang, T. et al., "A New Parallel Cut-Cell Cartesian CFD Code for Rapid Grid Generation Applied to In-Cylinder Diesel Engine Simulations," SAE Technical Paper 2007-01-0159, 2007, http://dx.doi.org/10.4271/2007-01-0159.
42. Han, Z., and Reitz, R.D., "Turbulence Modeling of Internal Combustion Engines Using RNG κ-ε Models," *Combustion Science and Technology* 106(4-6):267-295, 1995.
43. Amsden, A., "KIVA-3V: A Block-Structured KIVA Program for Engines with Vertical or Canted Valves," LA Report, 1997.
44. Chevillard, S., Colin, O., Bohbot, J., Wang, M. et al., "Advanced Methodology to Investigate Knock for Downsized Gasoline Direct Injection Engine Using 3D RANS Simulations," SAE Technical Paper 2017-01-0579, 2017, http://dx.doi.org/10.4271/2017-01-0579.
45. Colin, O., Benkenida, A., and Angelberger, C., "3D Modeling of Mixing, Ignition and Combustion Phenomena in Highly Stratified Gasoline Engines," *Oil Gas Science & Technlogy* 58(1):47-62, 2003.
46. Colin, O., and Truffin, K., "A Spark Ignition Model for Large Eddy Simulation Based on an FSD Transport Equation (ISSIM-LES)," *Proceeding of Combust Institute* 33(2):3097-3104, 2011.
47. De Bellis, V., Severi, E., Fontanesi, S., and Bozza, F., "Hierarchical 1D/3D Approach for the Development of a Turbulent Combustion Model Applied to a VVA Turbocharged Engine. Part II: Combustion Model," *Energy Procedia* 45:1027-1036, 2014, doi:10.1016/j.egypro.2014.01.108.

48. North, G.L., and Santavicca, D.A., "The Fractal Nature of Premixed Turbulent Flames," *Combustion Science and Technology* 72(4-6):215-232, 1990, doi:10.1080/00102209008951648.
49. Iafrate, N., Matrat, M. and Zaccardi, J.-M., "Numerical Investigations on Hydrogen-Enhanced Combustion in Ultra-lean Gasoline Spark-Ignition Engines," *International Journal of Engine Research*. August 2019, doi:10.1177/1468087419870688.
50. De Bellis, V., Bozza, F., and Tufano, D., "A Comparison Between Two Phenomenological Combustion Models Applied to Different SI Engines," SAE Technical Paper 2017-01-2184, 2017, http://dx.doi.org/10.4271/2017-01-2184.
51. Blizard, N., and Keck, J., "Experimental and Theoretical Investigation of Turbulent Burning Model for Internal Combustion Engines," SAE Technical Paper 740191, 1974, http://dx.doi.org/10.4271/740191.
52. Müller, C., "Investigation of a Pre-chamber Ignition System for the Application in an Ultra-Lean-Gasoline Hybrid Powertrain Engine", Ph.D. thesis, Institute for Combustion Engines (VKA), RWTH, Aachen, 2020.
53. Mastorakos, E., Allison, P., Giusti, A., De Oliveira, P. et al., "Fundamental Aspects of Jet Ignition for Natural Gas Engines," *SAE International Journal of Engines*, doi:10.4271/2017-24-0097.
54. Bozza, F., Teodosio, L., De Bellis, V., Fontanesi, S. et al., "A Refined 0D Turbulence Model to Predict Tumble and Turbulence in SI Engines," *SAE Int. J. Engines* 12(1):15-30, 2019, doi:10.4271/03-12-01-0002.
55. Bozza, F., De Bellis, V., Tufano, D., Malfi, E. et al., "A Quasi-Dimensional Model of Pre-Chamber Spark-Ignition Engines," SAE Technical Paper 2019-01-0470, 2019, http://dx.doi.org/10.4271/2019-01-0470.
56. Woschni, G., "Universally Applicable Equation for the Instantaneous Heat Transfer Coefficient in the Internal Combustion Engine," SAE Technical Paper 670931, 1967, http://dx.doi.org/10.4271/670931.
57. Lavoie, G., Heywood, J.B., and Keck, J., "Experimental and Theoretical Study of Nitric Oxide Formation in Internal Combustion Engines," *Combust. Sci. Technol* 1:313-326, 1970, doi:10.1080/00102206908952211.
58. Kaplan, J. and Heywood, J.. "Modeling the Spark Ignition Engine Warm-up Process to Predict Component Temperatures and Hydrocarbon Emissions," SAE Technical Paper 910302, 1991, 361-376, http://dx.doi.org/10.4271/910302.
59. Suckart, D., Linse, D., Schutting, E. et al., "Experimental and Simulative Investigation of Flame-Wall Interactions and Quenching in Spark-Ignition Engines," *Automot. Engine Technol* 2:25-38, 2017, doi:10.1007/s41104-016-0015-z.
60. Ishikawa, N., "Bulk and Wall Flame Quenching in Nonuniform Concentration Fields," *Combustion and Flame* 56(3):251-259, 1984, doi:10.1016/0010-2180(84)90059-2.
61. Kwon, H., and Min, K., "Modified One-Step Reaction Equation for Modeling the Oxidation of Unburned Hydrocarbons in Engine Conditions," *International Journal of Automotive Technology* 11:637-650, 2010, doi:10.1007/s12239-010-0076-3.

Acknowledgements

This project has received funding from the European Union's Horizon 2020 research and innovation programme under grant agreement No 724084 (https://h2020-eagle.eu/). The project main objective is the experimental and numerical investigation of an ultra-lean combustion concept, applied to a novel engine architecture fitted in a hybrid powertrain. The most ambitious goal is the attainment of very reduced fuel consumption and NOx and CO_2 emissions, compared to a conventional SI engine.

Acronyms

0D-1D-3D - Zero-one-three-dimensional
aTDC - After firing top dead center
bTDC - Before top dead center
CAD - Crank angle degree
CFD - Computational fluid dynamics
CO - Carbon monoxide
CO_2 - Carbon dioxide
CoV - Coefficient of variation
HP - High pressure
ICE - Internal combustion engine
IMEP - Indicated mean effective pressure
IS - Indicated specific
LP - Low pressure
MC - Main-chamber
MFB - Mass fraction burned
NO_X - Nitrogen oxides
PC - Pre-chamber
RMSE - Root mean squared error
RNG - Renormalization group
SA - Spark advance
SCE - Single cylinder engine
SI - Spark ignition
TDC - Top dead center
uHC - Unburned hydrocarbon
VVA/VVT - Variable valve actuation / timing
WLTC - Worldwide harmonized light vehicle test cycle

Symbols

A_L, A_T - Laminar / turbulent flame area
c_{jet} - Fresh charge entrainment multiplier
c_{trans} - Laminar turbulent transition multiplier
$_{Cwc}$ - Wall combustion tuning multiplier
c_{wrk} - Wrinkling multiplier
D_3 - Fractal dimension
k - Turbulent kinetic energy

K - Mean flow kinetic energy
L_{min}*, *L_{max} - Minimum / maximum flame front wrinkling scale
M - Mass
r_{crit} - PC critical radius for MC combustion start
S_L*, *S_T - Laminar / turbulent flame speed
T - Tumble angular momentum/Temperature
t - Time
u' - Turbulence intensity

Greeks

Λ_T - Taylor length scale
λ - Relative air/fuel ratio
ρ - Density
τ - Entrainment characteristic time

Subscripts

10 / 50 / 90 - Referring to 10 / 50 / 90% of mass fraction burned
b - Burned
entr - Entrainment
F - Related to flame
fractal - Related to fractal approach
jet - Related to turbulent jet
MC - Related to main-chamber
PC - Related to pre-chamber
u - Unburned

Superscripts

. - Temporal derivative

ISSN 0148-7191